Princeton Plasma Physics Laboratory

PPPL- 4547

PPPL- 4547

Some Considerations and Techniques for the Predictive Simulation of Global Instabilities in Tokamaks

S.C. Jardin

September, 2010

Prepared for the U.S. Department of Energy under Contract DE-AC02-09CH11466.

Princeton Plasma Physics Laboratory
Report Disclaimers

Full Legal Disclaimer

Trademark Disclaimer

PPPL Report Availability

Princeton Plasma Physics Laboratory:

http://www.pppl.gov/techreports.cfm

Office of Scientific and Technical Information (OSTI):

http://www.osti.gov/bridge

Related Links:

U.S. Department of Energy

Office of Scientific and Technical Information

Fusion Links

Some considerations and techniques for the predictive simulation of global instabilities in tokamaks

S. C. Jardin
Princeton Plasma Physics Laboratory, Princeton NJ 08540

Abstract

This is a write-up of a lecture given at the Fourth ITER International Summer School held at the IFS, U. Texas in June 2010. A simple rigid plasma model is used to show that axisymmetric plasma instabilities (in two-dimensions) will occur on a resistive timescale and do not depend on the plasma mass. This is the justification for ignoring the inertial term in two-dimensional studies of plasma shape control and vertical stability. In three dimensions, it is not normally possible to ignore the inertial terms when computing plasma instabilities. This results in a stiff system of equations (with multiple timescales) in which the driving terms causing plasma instabilities are small compared with the stable compressive terms. Techniques are described for implicit time integration and for representing the vector fields in a way to facilitate obtaining accurate solutions for plasma instabilities when a strong background magnetic field is present.

I. Introduction

The macroscopic dynamics of instabilities in tokamaks are well described by the magnetohydrodynamic (MHD) equations, which are obtained by integrating velocity moments of the Boltzmann equations for the electrons and ions over velocity space and combining this with the low-frequency Maxwell Equations [1,2]. In this paper, we are concerned with techniques for solving these equations numerically to predict the onset and saturation amplitude of instabilities in tokamaks.

There are many simpler sets of equations that make additional approximations to more efficiently describe a given tokamak instability. Some of these, are called “reduced MHD” [3], or “the island evolution equation”[4], or “the Porcelli sawtooth model”[5], etc. These simpler, model equation sets, are extremely useful for understanding the basic physics of certain instabilities. However, the approach we discuss here is that of the SciDAC [6] project, “The Center for Extended Magnetohydrodynamic Modeling” [7], which seeks to solve the full 3D MHD equations without making other approximations and keeping all the geometric detail. This is much more computationally intensive than applying the simpler models, but can lead to new discoveries of phenomena that are absent in the simplified models, and can provide quantitative results for direct comparison with experiments over a wide range of parameters.

In Section II we introduce a simple “rigid” plasma model in 2D in order to show that plasma dynamics that enter 2D plasma control and instability calculations do not depend on the plasma mass. This

justifies the expansion used in Section III to remove the inertial terms from the MHD equations (and thus the Alfven wave characteristics) in order to obtain a description of the resistive time scale plasma dynamics in 2D that is free of the stiffness that would be present if the Alfven wave dynamics were present. This simplification is generally not possible in 3D, and in Section IV we describe several essential techniques that enable solving the 3D MHD equations for plasma instabilities in a strongly magnetized plasma over long timescales. In Section V we summarize the principle points made in the paper.

II. Timescales in 2D and the rigid plasma model

All modern tokamaks with elongated cross sections are unstable to a "vertical instability" which is an axisymmetric nearly rigid motion of the plasma column [8]. In order to understand the timescales involved in this instability, let us first consider a linear rigid plasma model which is subject to the vertical instability in the presence of a resistive coil (or other conductor). Let the vertical location of the plasma be denoted by Z_P and the current in the resistive coil be I_C. These are infinitesimal quantities that are assumed to vary as the real part of $\exp[i\omega t]$. The equation of motion for the plasma can then be written:

$$-m\omega^2 Z_P = \left(I_P M'_{CP}\right) I_C + \left(I_P B'_R\right) Z_P \quad . \tag{1}$$

Here we have introduced some equilibrium quantities and denoted the plasma mass by m, the plasma current by I_P, the derivative of the mutual inductance between the plasma and the coil by M'_{CP}, and the derivative of the external radial field component with respect to Z by B'_R. The circuit equation for the resistive coil with resistivity R and self inductance L that is interacting inductively with the rigid plasma can be written:

$$i\omega L I_C + R I_C + i\omega\left(M'_{CP} I_P\right) Z_P = 0 \ . \tag{2}$$

We can introduce the plasma velocity $V_P = i\omega Z_P$ and rewrite Eqs. (1) and (2) as the generalized eigenvalue problem for the mode frequency:

$$\omega \begin{bmatrix} i & 0 & 0 \\ 0 & im & 0 \\ iM'_{CP} I_P & 0 & iL \end{bmatrix} \bullet \begin{bmatrix} Z_P \\ V_P \\ I_C \end{bmatrix} = \begin{bmatrix} 0 & 1 & 0 \\ I_P B'_R & 0 & I_P M'_{CP} \\ 0 & 0 & -R \end{bmatrix} \bullet \begin{bmatrix} Z_P \\ V_P \\ I_C \end{bmatrix}. \tag{3}$$

Equation (3) has 3 roots. It is convenient to define the real quantities $\gamma_R \equiv R/L$, $\omega_0^2 \equiv I_P B'_R / m$, $\omega_s^2 \equiv \left(I_P M'_{CP}\right)^2 / mL$ corresponding to the inverse resistive decay time of the wall, the square of the growth rate of the unstabilized vertical instability, and the normalized stabilizing force of the wall. These must satisfy $\omega_0^2 < \omega_S^2$ and $\gamma_R^2 \ll \omega_0^2$.

In terms of these quantities, the three roots of Eq. (3) are given by:

$$\omega_{1,2} = \pm\left[\omega_S^2 - \omega_0^2\right]^{1/2} + i\frac{\gamma_R}{2}\frac{\omega_S^2}{\left(\omega_S^2 - \omega_0^2\right)}, \qquad \omega_3 = -i\gamma_R\frac{\omega_0^2}{\left(\omega_S^2 - \omega_0^2\right)} \ . \tag{4}$$

It is clear from Eq. (4) that there are two distinct timescales in the problem. Roots #1 and #2 in Eq. (4) are high frequency oscillatory modes that are slowly damped by the wall resistivity. Root #3 is the residual slowly growing vertical instability, sometimes called the axisymmetric resistive wall mode. The vertical instability is thus stabilized by a two-tier approach. A conducting metallic structure, normally the vacuum vessel, provides a passive stabilizing force that satisfies $\omega_S^2 > \omega_0^2$. This slows the instability growth rate down to the L/R time of the vessel, and then an active feedback system using the poloidal field coils is used to provide complete stability.

III. Nonlinear simulation of deformable plasmas in 2D

The fact that the unstable motion for this vertical instability occurs only on the resistive time scale leads to great simplification in the MHD equations we use to describe it. Consider the following set of basic resistive MHD equations in 2D:

Faraday's law for the evolution of the magnetic field:

$$\frac{\partial \mathbf{B}}{\partial t} = -\nabla \times \mathbf{E} \, . \tag{5}$$

The momentum equation:

$$nM_i\left(\frac{\partial \mathbf{V}}{\partial t} + \mathbf{V} \bullet \nabla \mathbf{V}\right) + \nabla p = \mathbf{J} \times \mathbf{B} \ . \tag{6}$$

The generalized Ohm's law equation:

$$\mathbf{E} + \mathbf{V} \times \mathbf{B} = \eta \mathbf{J} \ . \tag{7}$$

The internal energy equation:

$$\frac{3}{2}\frac{\partial p}{\partial t} + \nabla \bullet \left(\frac{3}{2} p\mathbf{V} + \mathbf{q}\right) = -p\nabla \bullet \mathbf{V} + \eta J^2 \, . \tag{8}$$

Definition of the current density, valid at low frequencies:

$$\mathbf{J} = \mu_0 \nabla \times \mathbf{B} \, . \tag{9}$$

Circuit equation for each conductor, including the inductive coupling to the plasma:

$$\frac{d}{dt}\left[L_i I_i + \sum_{i \neq j} M_{ij} I_j + \int_P J_\phi G(\mathbf{R_i}, \mathbf{R}) \mathbf{dR} \right] + R_i I_i = V_i \ . \tag{10}$$

We have denoted the Green's function for an axisymmetric current source in Eq. (10) by $G(\mathbf{R}, \mathbf{R}')$, and the integral is over the plasma volume. This set of equations contains both the ideal MHD (or Alfven) time scales and the resistive time scales. In order to remove the ideal MHD timescales and obtain a set of equations that is suitable for the slower resistive timescale, we introduce an ordering parameter $\varepsilon \ll 1$ that is the order of the plasma and the wall resistivity, and look for solutions where the velocity and all time derivatives are small, of order ε. Formally, we take the ordering:

$$\frac{\partial}{\partial t} \sim \mathbf{V} \sim \mathbf{E} \sim V_i \sim \eta \sim R_i \sim \varepsilon \ . \tag{11}$$

When the ordering of Eq. (11) is applied to Eqs. (5)-(10), all but one of the equations remains unchanged, merely picking up a factor of ε in each term which then cancel. The exception is the momentum equation, Eq. (6), which becomes

$$\varepsilon^2 n M_i \left(\frac{\partial \mathbf{V}}{\partial t} + \mathbf{V} \bullet \nabla \mathbf{V}\right) + \nabla p = \mathbf{J} \times \mathbf{B} \ . \tag{12}$$

This ordering allows us to replace Eq. (6) by the equilibrium equation, valid to second order in ε:

$$\nabla p = \mathbf{J} \times \mathbf{B} \ . \tag{13}$$

Thus, the set of equations given by Eqs. (5), (13), (7), (8), (9), and (10) are accurate to second order in the small parameter ε and are free from the fast Alfven wave timescales. (Note: an additional "surface averaging" of the energy equation, Eq. (8), can be performed to eliminate the fast timescale associated with the large thermal conductivity, but we will not consider that further here.) The equations can then be cast in a moving coordinate system where the toroidal flux is used as the independent variable [2]. There are two approaches to incorporating the equilibrium constraint, Eq. (13) into this set of equations that have been implemented into production codes.

In the Grad-Hogan method [2,9,10], every time step is split into two parts. In the first part, the adiabatic variables, namely the plasma safety factor and entropy density, as well as the poloidal flux at the conductors, are advanced from time t to time $t + \delta t$. In the second part, these adiabatic variables are held fixed while we solve the appropriate form of the equilibrium equation, where the "free functions" have been expressed in terms of the adiabatic variables. The individual coil and conductor currents will change during this part of the time step in order to keep the poloidal flux fixed at each coil location and at the plasma magnetic axis. This part of the time step effectively determines the absolute motion of the toroidal flux surfaces relative to a fixed frame.

J. B. Taylor [11] suggested an alternative to the Grad–Hogan method that does not require solving the equilibrium equation with the adiabatic constraints. His approach involves solving for the velocity field $\mathbf{V}$, which when inserted into the field and pressure evolution equations, Eqs. (5), and (8), will result in the equilibrium equation, Eq. (13), continuing to be satisfied as time evolves. An implementation of this approach [12] uses the accelerated steepest descent algorithm which involves obtaining the velocity from the residual equation,

$$\frac{\partial \mathbf{V}}{\partial t} + \frac{1}{\tau}\mathbf{V} = D\left[\mathbf{J}\times\mathbf{B} - \nabla p\right]. \tag{14}$$

By choosing the proportionality and damping factors, D and τ appropriately, the system can be kept arbitrarily close to an equilibrium state as it evolves. This is equivalent to applying the dynamic relaxation method [2] to the plasma equilibrium problem.

These "1 ½ D Free boundary transport codes" are now routinely used to simulate shaping algorithms, calculate vertical stability margins, and calculate flux-swing requirements for tokamaks [13-20].

IV. Simulation and control of instabilities in 3D

In describing 3D tokamak instabilities, it is normally not possible to use the ordering of the last section and replace the momentum equation, Eq. (6), by the equilibrium equation, Eq. (13). This is because of the existence of intermediate timescales that are proportional to fractional powers of the resistivity [21] and the importance of flows in determining 3D stability. Three dimensional MHD instabilities of interest include the sawtooth oscillation, kink and ballooning modes, tearing modes, edge localized modes (ELMs) and resistive wall modes (RWM). The latter are the 3D analogue of the vertical instability. The instabilities with the slowest growth rates are the most challenging to simulate because of the problems of accurately computing the small driving force and the associated long integration times. This has led to the development of fully implicit time integration methods [22,23] and to the use of high-order finite elements and a representation for the velocity field that permits plasma motions that do not compress the toroidal field to a high order of accuracy.

It has been shown by several authors [23-27] that a stable implicit numerical time stepping algorithm that is second order accurate in time, now known as the method of differential approximation, can be obtained by replacing Eq. (6) by the following equation, and then by applying centered time differences and either centered space differences or finite elements:

$$\left\{n - \theta^2\left(\delta t\right)^2 L\right\}\frac{\partial \mathbf{V}}{\partial t} + n\mathbf{V}\bullet\nabla\mathbf{V} + \nabla p + \nabla\bullet\mathbf{\Pi} = \mathbf{J}\times\mathbf{B}\ . \tag{15}$$

This is followed by an implicit time advance for the magnetic field, pressure, and density using the advanced time velocity. Here we have introduced the implicit parameter θ, where $1/2 \le \theta \le 1$ for numerical stability, δt is the time-step, and L is the linear ideal MHD operator [28]:

$$L\{\mathbf{V}\} = \{\nabla\times[\nabla\times(\mathbf{V}\times\mathbf{B})]\}\times\mathbf{B} + (\nabla\times\mathbf{B})\times[\nabla\times(\mathbf{V}\times\mathbf{B})] + \nabla(\mathbf{V}\bullet\nabla p + \gamma p\nabla\bullet\mathbf{V}) \quad . \tag{16}$$

In describing unstable motions of a low $\beta \equiv 2\mu_0 p / B^2$ plasma with a strong background magnetic field, such as a tokamak, it is essential to employ high-accuracy spatial representations so that numerical errors associated with computation of the stable modes do not interfere with the computation of the unstable modes. One approach [23] is to represent the velocity and magnetic fields by their cylindrical coordinate projections and use high-order finite elements to accurately compute the product terms. Another approach [22] is to represent the velocity and magnetic fields in terms of stream functions and potentials that exhibit analytic cancelations in the asymptotic large-toroidal-field limit.

This second approach is illustrated here. Consider the following forms for the velocity and magnetic field vectors:

$$\mathbf{V} = R^2\nabla U\times\nabla\varphi + \omega R^2\nabla\varphi + R^{-2}\nabla_\perp\chi \quad , \tag{17}$$

$$\mathbf{B} = \nabla\psi\times\nabla\varphi - \nabla\frac{\partial f}{\partial\varphi} + F^*\nabla\varphi \quad . \tag{18}$$

Here, $F^* \equiv (F_0 + R^2\nabla^2 f)$. In this representation, (R,φ,Z) are standard cylindrical coordinates, the velocity is represented by the three scalar fields (U,ω,χ), and the magnetic field is represented by the two scalar fields (ψ, f) and the constant F_0, which represents the strong externally imposed toroidal field. This representation of the magnetic field is totally general and intrinsically divergence free. We have introduced the symbol $\nabla_\perp$ to indicate the 2D gradient operator in the (R,Z) plane. The first term in the velocity represents motion within a 2D poloidal plane (at a fixed toroidal angle) that does not compress the background toroidal field, the second term represents the motion in the toroidal direction, and the third term, which is normally very small, represents compressible motion within the poloidal plane. Note that it is orthogonal to the first term in that the inner product of those two terms vanishes when integrated over the torus.

A plasma instability will develop in such a way as to not compress the strong toroidal field, as it is energetically unfavorable to do so. It is important that the discrete representation that one uses to represent the vector fields allows this class of motion to high accuracy. To see that the first velocity term does not, in fact, compress the background toroidal field, we can substitute $\mathbf{V} = R^2\nabla U\times\nabla\varphi$ and $\mathbf{B} = F_0\nabla\varphi$ into the ideal-MHD parts of Eq. (5) and (7) (i.e. with η=0) and compute the toroidal component:

$$\begin{aligned}\nabla\varphi\bullet\frac{\partial\mathbf{B}}{\partial t} &= \nabla\varphi\bullet\nabla\times\left[\mathbf{V}\times\mathbf{B}\right] \\ &= \nabla\varphi\bullet\nabla\times\left[\left(R^2\nabla U\times\nabla\varphi\right)\times\left(F_0\nabla\varphi\right)\right] \\ &= F_0\nabla\bullet\left[\nabla\varphi\times\nabla U\right] \\ &= 0\end{aligned} \tag{19}$$

We are thus able to eliminate this possibly large error term associated with anomalous compression of the externally imposed toroidal field analytically from the equations, resulting in a large increase in accuracy. The velocity field associated with this first term always dominates over that associated with the third term in Eq. (17) when computing plasma instabilities.

When using a velocity representation such as that in Eq. (17), it is also important what projections one takes of the momentum equation. Ideally, these projections will isolate the motion that compresses the toroidal field to a single equation which does not interfere with the others, at least to lowest order. When applying the Galerkin finite element method [29], one operates on the momentum equation with a differential operator, multiplies by the finite element ν_i, and integrates over all space to obtain the weak form of the equation. Consider the following annihilation operators applied to the modified momentum equation, Eq. (15), and then integrated by parts.

$$\iint d^2R\,\nu_i\nabla\varphi\bullet\nabla_\perp\times R^2(17) \quad\rightarrow\quad \iint d^2R\,R^2\nabla_\perp\nu_i\times\nabla\varphi\bullet(17) \tag{20a}$$

$$\iint d^2R\,\nu_i R^2\nabla\varphi\bullet(17) \quad\rightarrow\quad \iint d^2R\,\nu_i R^2\nabla\varphi\bullet(17) \tag{20b}$$

$$-\iint d^2R\,\nu_i\nabla_\perp\bullet R^{-2}(17) \quad\rightarrow\quad \iint d^2R\,R^{-2}\nabla_\perp\nu_i\bullet(17) \tag{20c}$$

The boundary terms from the integration by parts are assumed to vanish here. For a uniform density plasma, these are seen to approximately project out each of the three terms in the velocity as represented in Eq. (17). In addition, by comparing the integrands on the right in Eq. (20) with the form of the velocity in Eq. (17), we see that after the integration by parts, these projection operators are equivalent to taking the inner product of the momentum equation, Eq. (15), separately with each of the three terms in the velocity field, but with the trial function ν_i replacing each of the three scalars (U,ω,χ). This property leads to an energy-conserving set of discrete equations and to self-adjoint energy terms, called partial energy terms, being introduced in the implicit time advance. By using only Eq. (20a) or only Eq. (20a) and (20b) we can obtain energy conserving subsets of reduced equations as well.

Similar projections and integrations are performed with the magnetic field advance equation, with the projection operators being given by:

$$\iint d^2R\,\nu_i\nabla\varphi\bullet\nabla_\perp\times(5) \quad\rightarrow\quad \iint d^2R\,\nabla_\perp\nu_i\times\nabla\varphi\bullet(5)\ , \tag{21a}$$

$$\iint d^2R\, \nu_i \nabla\varphi \bullet (5) \quad \rightarrow \quad \iint d^2R\, \nu_i \nabla\varphi \bullet (5) \quad . \tag{21b}$$

As in the discussion following Eq. (20), if we compare the integrands on the right in Eq. (21) with the form of the magnetic field in Eq. (18), we see that these projection operators are equivalent to taking the inner product of the magnetic field evolution equation, Eq. (5), with the first and third terms in the magnetic field, but with the trial function ν_i replacing the scalar quantities ψ and *F**. In this case, there is no need to take the third projection, which would be

$$-\iint d^2R\, \nu_i \nabla \bullet (5) \quad \rightarrow \quad \iint d^2R\, \nabla \nu_i \bullet (5)\ , \tag{23c}$$

since the divergence constraint on the magnetic field assures that this is satisfied.

Recent application of these codes includes modeling of the sawtooth activity [30-32], both linear [33,34] and nonlinear [35,36] properties of Edge localized modes, the response of the plasma to resonant magnetic perturbations [37-39], and the growth and stabilization of tearing modes [40]. We are also applying these codes to calculate the forces on the vacuum vessel when the plasma undergoes a major disruption [41-44].

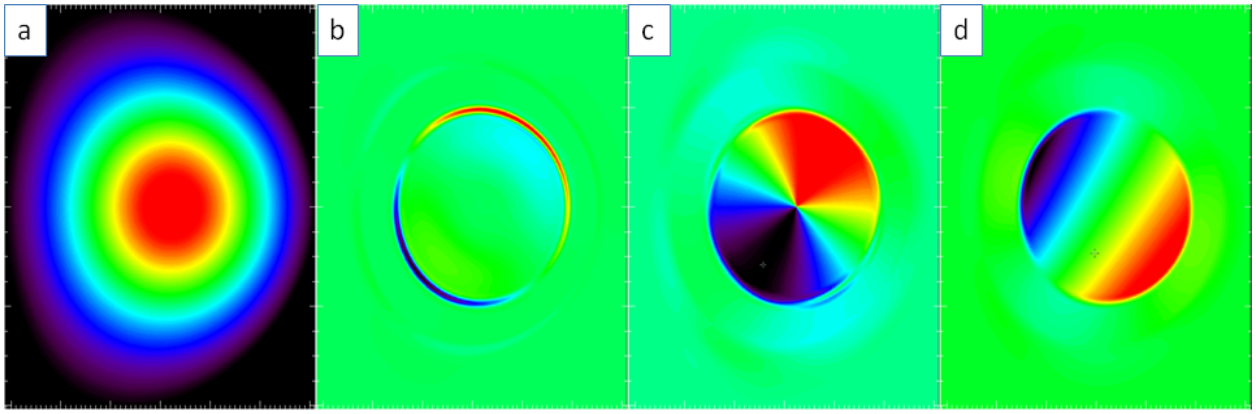

Figure 1: (a) Poloidal flux in equilibrium configuration; (b) Perturbed toroidal current density; (c) Perturbed velocity normal to the equilibrium flux surfaces; (d) Perturbed "U" scalar from Eq. (17).

An example of a calculation performed using the techniques discussed in this paper is shown in Figure 1. The M3D-*C*^{1} code [45] was used to calculate a resistive tearing instability in a standard tokamak configuration. The equilibrium was defined by a plasma with an outer boundary shape of dimensionless major radius R=1, aspect ratio a/R=0.313, ellipticity 1.3 and triangularity 0.2. The central β was $2p_0 / B_0^2 = 1.2\%$. The safety factor ranged from $0.6 < q < 6.0$. Using standard normalizations [45], we take $B_0 = 1$ and the plasma resistivity to be a constant: $\eta = 10^{-7}$. For this linear calculation, we assume the toroidal dependence to vary as $e^{in\varphi}$ and take the real part. The equilibrium is unstable to a tearing instability that is localized around the $q = 1$ surface. We show the equilibrium configuration and several components of the computed unstable linear eigenmode in Figure 1. For this case, the maximum value

of the potential term in the velocity representation in Eq. (17), χ (not shown), was over an order of magnitude smaller than the maximum value of U, shown in Figure 1d. This illustrates that this velocity decomposition was successful for calculating this mode. This eigenmode was computed as an initial value problem with a time-step of $\Delta t = 1.0$ (in these normalized units) which is several orders of magnitude larger than what would be required were a fully explicit method applied to the 3D MHD equations.

V. Summary

In two dimensions, the motion of a wall stabilized tokamak plasma is well described by a reduced system of equations in which the inertial terms are removed from the momentum equation. This removes the Alfven wave timescales from the equations and leaves only the much slower dissipative time scales. Several 2D codes take exist which solve the 2D MHD equations on the dissipative time scale and are in wide use today. In three dimensions, it is not normally possible to ignore the inertial terms. The resulting multiple timescales and associated weak forces causing instability make 3D simulations much more difficult. Techniques are described for implicit time integration and for obtaining accurate solutions when a strong background magnetic field is present. Key to this is a representation of the velocity field where the plasma motion in the poloidal plane that does not compress the external magnetic field is isolated and solved for in a separate equation. An example is presented of the computation of a typical tearing instability in a high field tokamak that confirms that the implicit algorithm presented and the form of the vector fields given in Eqs. (17) and (18) are effective for computing this class of tokamak instabilities.

Acknowledgements

Work supported by the CEMM and SWIM SciDAC grants and US DOE Contract NO. DE-AC02-76CH03073

References

[1] Braginski, S. I. 1966. Transport processes in a plasma. In *Review of Plasma Physics, Vol. I*, ed. M. A. Leontovich, 205-3111. New York: Consultants Bureau.

[2] Jardin, S. C. 2010. *Computational Methods in Plasma Physics*. Boca Raton, FL: Taylor & Francis

[3] Strauss, H. R. 1976. Nonlinear 3-dimensional magnetohydrodynamics of noncircular tokamaks. *Phys. Fluids* **19**:134

[4] Rutherford, P. H. 1973. Nonlinear growth of tearing modes. *Phys. Fluids* **16**:1903-8

[5] Porcelli, F, D. Boucher, M.N. Rosenbluth. 1996. Model for the sawtooth period and amplitude. *Plasma Physics and Controlled Fusion.* **38:**2163-86

[6] http://www.scidac.org

[7] http://w3.pppl.gov/CEMM

[8] Jardin, S. C. and D. Larrabee. 1982. Feedback stabilization of rigid axisymmetric modes in tokamaks. *Nuclear Fusion.* **22**:1095-98

[9] Grad H. and J. Hogan. 1970. Classical diffusion in a tokamak. Phys. Rev. Lett. **24**:1337.

[10] Blum J. and J. LeFoll. 1984. Plasma equilibrium evolution at the resistive diffusion timescale. J. Comp. Phys. Reports **1**:465-494.

[11] Taylor, J. B., 1975. Private communication.

[12] Jardin, S, N. Pomphrey, J. DeLucia. 1986. Dynamic modeling of transport and positional control of tokamaks. *J. Comput. Phys*. **66**:481-507.

[13] Marcus, F.B., S. C. Jardin, F. Hofmann, 1985. Controlled evolution of highly elongated tokamak plasmas. *Phys. Rev. Lett***. 55**:2289-2292

[14] Jardin, S. C., J. Delucia, M. Okabayashi, et al, 1987. Modeling of post-disruptive plasma loss in the Princeton-beta-experiment. *Nucl. Fusion* **27**:569-578

[15] Pomphrey, N., S. C. Jardin, D. J. Ward. 1989. "Feedback stabilization of the axisymmetric instability of a deformable tokamak plasma", Nucl. Fus. 29: 465-473

[16] Weiner, R. , S. C. Jardin, N. Pomphrey. 1989. Stability of elongated cross-section tokamaks to axisymmetric even poloidal mode number deformations. *Phys. Fluids B*. **12:**2349-2352

[17] Marcus, F. B., F. Hofmann, S. C. Jardin. 1990. Simulations of control, perturbation, displacement and disruption in highly elongated tokamak plasmas. *Nucl. Fus*. **30**:1511-1521.

[18] Hofmann, F., S. C. Jardin. 1990. Plasma shape and position control in highly elongated tokamaks. *Nucl. Fus*. **30**:2013-2022

[19] Jardin, S. C., M. G. Bell, N. Pomphrey. 1993. TSC simulation of ohmic discharges in TFTR. *Nucl. Fus.* **33:**371-382

[20] Jardin, S. C., C. E. Kessel, N. Pomphrey. 1994. Poloidal flux linkage requirements for the International Thermonuclear Experimental Reactor. *Nucl. Fus.* **34**:1145-1160.

[21] Furth, H, J. Killeen, and M. Rosenbluth. 1960. Finite-resistivity instabilities of a sheet pinch. *Phys. Fluids* **6**:459-84

[22] Breslau, J., N. Ferraro, S. C. Jardin. 2009. Some properties of the M3D-C^1 form of the 3D MHD equations. *Phys. Plasma* **16**:092503

[23] Sovinec, C., A. H. Glasser, T. Gianakon, et al. 2004. Nonlinear magnetohydrodynamics simulation using high-order finite elements. *J. Comput. Phys* **195**:355-386

[24] Caramana, E. 1991. Derivation of implicit difference schemes by the method of differential approximation. *J. Comput. Phys*. **96**:484-93

[25] Jardin,S. C., J. Breslau, N. Ferraro. 2007. A high-order implicit finite element method for integrating the two-fluid magnetohydrodynamic equations in two dimensions.J. *Comput. Phys*. **226**:2146

[26] Ferraro, N. and S. Jardin. 2006. Finite element implementation of Braginskii's gyroviscous stress with application to the gravitational instability. *Phys. Plasmas* **13**:092101

[27] Ferraro, N. and S. Jardin, 2009 Calculations of Two-Fluid Magnetohydrodynamic Axisymmetric Steady States. *J. Comput. Phys*. **228**:7742-70

[28] Bernstein, I, E. Frieman, M. Kruskal, and M. Kulsrud, 1958, An energy principle for hydromagnetic stability problems. *Proc. Royal Soc. London Ser. A* **244**:17

[29] Strang, C. and C. J. Fix. 1973 *An Analysis of the Finite Element Method*. Englewood Cliffs, NJ: Prentice-Hall

[30] Breslau, J. A., S. C. Jardin, W. Park. 2007. Three-dimensional modeling of the sawtooth instability in a small tokamak. *Phys. Plasmas* **14**:056105

[31] Breslau, J. A., C. R. Sovinec, S. C. Jardin. 2008. An improved tokamak sawtooth benchmark for 3D nonlinear MHD. *Comm. in Comput . Physics* **4**:647-658.

[32] Kim, C. C. and the NIMROD Team. 2008. Impact of velocity space distribution on hybrid kinetic-magnetohydrodynamic simulation of the (1,1) mode. *Phys. Plasmas* **15**:72507.

[33] Burke, B. J, S. E. Kruger, C. C. Hegna, P. Zhu, P .B. Snyder, C. R. Sovinec, and E. C. Howell. 2010. Edge localized linear ideal magnetohydrodynamic instability studies in an extended-magnetohydrodynamic code. *Phys. Plasmas*. **17**:032103

[34] Ferraro, N.M., S. C. Jardin, and P. Snyder. 2010. Ideal and resistive edge stability calculations with M3D-C1. submitted to *Phys. Plasmas.* [http://w3.pppl.gov/cemm/Project/ELMbenchmark.pdf]

[35] Sugiyama, L.2009. Magnetic X-points, stochasticity, and Edge Localized Modes. *J. Phys: Conf. Series* **180**:012060

[36] Sugiyama,L, and H. Strauss. 2010. ELMs, Magnetic X-points, and Chaotic Fields. to appear in *Phys Plasmas*

[37] Izzo, V. A. and I. Joseph. 2008. RMP enhanced transport and rotational screening in simulations of DIII-D plasmas. *Nuclear Fusion* **48**(11) in Proc. 22nd Int. IAEA Conf. Generva TH/P4-19

[38] Strauss, H. R., and L. Sugiyama. 2008. MHD Simulation of Resonant Magnetic Perturbations and ELMs. Proc. 22nd Int. IAEA Conf. Geneva TH/2-1Rb

[39] Strauss, H. R., L. Sugiyama, G. Y. Park. 2009. Extended MHD simulation of resonant magnetic perturbations. *Nuclear Fusion* **49**:055025

[40] Jenkins, T. G., S. E. Kruger, et al. 2010. Calculating electron cyclotron current drive stabilization of resistive tearing modes in a nonlinear magnetohydrodynamic model. *Phys. Plasmas* **17**:012502.

[41] Izzo, V. A., P. B. Parks, L. Lao. 2009. DIII-D and ITER rapid shutdown with radially uniform deuterium delivery. *Plasma Physics and Controlled Fusion* **51**:105004.

[42] Izzo, V. A., D. G. Whyte, et al. 2008. Magnetohydrodynamic simulations of massive gas injection into Alcator C-Mod and DIII-D plasmas. *Phys. Plasmas* **15**:056109.

[43] Paccegnella, R, H. R. Strauss, and J. Breslau. 2009. 3D MHD VDE and disruption simulations of tokamak plasmas including some ITER scenarios. *Nucl. Fus.* **49:**035003

[44] Strauss, H.R., R. Paccagnella, and J. Breslau. 2010. Kink modes produced wall forces during ITER disruptions. submitted to *Phys. Plasmas*. http://w3.pppl.gov/cemm/Project/strauss-2010.pdf

[45] Jardin, S. C., N. Ferraro, X. Luo, UJ. Chen, J. Breslau, K. E. Jansen, and M. S. Shephard. 2008. The M3D-C^1 approach to simulating 3D 2-fluid magnetohydrodynamics in magnetic fusion experiments". *Journal of Physics: Conference Series* **125**: 012044

The Princeton Plasma Physics Laboratory is operated
by Princeton University under contract
with the U.S. Department of Energy.

Information Services
Princeton Plasma Physics Laboratory
P.O. Box 451
Princeton, NJ 08543

Phone: 609-243-2245
Fax: 609-243-2751
e-mail: pppl_info@pppl.gov
Internet Address: http://www.pppl.gov